Osteoarthritis and Cartilage Open 6 (2024) 100436

Contents lists available at ScienceDirect

Osteoarthritis and Cartilage Open

journal homepage: www.elsevier.com/journals/osteoarthritis-and-cartilage-open/2665-9131

Brief Report

Dual energy computed tomography cannot effectively differentiate between calcium pyrophosphate and basic calcium phosphate diseases in the clinical setting

Mohamed Jarraya [a,*], Olivier Bitoun [a], Dufan Wu [a], Rene Balza [a], Ali Guermazi [b], Jamie Collins [c], Rajiv Gupta [a], Gunnlaugur Petur Nielsen [d], Elias Guermazi [e], F. Joseph Simeone [a], Patrick Omoumi [f], Christopher M. Melnic [g], Seonghwan Yee [a]

[a] Department of Radiology, Massachusetts General Hospital, Harvard Medical School, Boston, MA, USA
[b] VA Boston Healthcare, Boston University School of Medicine, Boston, MA, USA
[c] Orthopedic and Arthritis Center for Outcomes Research, Department of Orthopedic Surgery, Brigham and Women's Hospital, USA
[d] Department of Pathology, Massachusetts General Hospital, Harvard Medical School, Boston, MA, USA
[e] Boston University, Boston, MA, USA
[f] Centre Hospitalier Universitaire Vaudois (CHUV), Lausanne, Switzerland
[g] Department of Orthopedics, Massachusetts General Hospital, Harvard Medical School, Boston, MA, USA

ARTICLE INFO

Handling Editor: Professor H Madry

Keywords:
Osteoarthritis
Dual energy
CT
Crystal
Calcium phosphate

ABSTRACT

Background: Recent reports suggested that dual-energy CT (DECT) may help discriminate between different types of calcium phosphate crystals *in vivo*, which would have important implications for the characterization of crystal deposition occurring in osteoarthritis.
Purpose: Our aim was to test the hypothesis that DECT can effectively differentiate basic calcium phosphate (BCP) from calcium pyrophosphate (CPP) deposition diseases.
Methods: Discarded tissue after total knee replacement specimens in a 71 year-old patient with knee osteoarthritis and chondrocalcinosis was scanned using DECT at standard clinical parameters. Specimens were then examined on light microscopy which revealed CPP deposition in 4 specimens (medial femoral condyle, lateral tibial plateau and both menisci) without BCP deposition. Regions of interest were placed on post-processed CT images using Rho/Z maps (Syngo.via, Siemens Healthineers, VB10B) in different areas of CPP deposition, trabecular bone BCP (T-BCP) and subchondral bone plate BCP (C-BCP).
Results: Dual Energy Index (DEI) of CPP was 0.12 (SD = 0.02) for reader 1 and 0.09 (SD = 0.03) for reader 2, The effective atomic number (Z_{eff}) of CPP was 10.83 (SD = 0.44) for reader 1 and 10.11 (SD = 0.66) for reader 2. Nearly all DECT parameters of CPP were higher than those of T-BCP, lower than those of C-BCP, and largely overlapping with Aggregate-BCP (aggregate of T-BCP and C-BCP).
Conclusion: Differentiation of different types of calcium crystals using DECT is not feasible in a clinical setting.

1. Introduction

Over the past few years, a number of publications have discussed the potential role of dual-energy CT (DECT) [1–4] and even multi-energy CT [5–7] to characterize calcium crystal deposition in and around the joints, and particularly to differentiate basic calcium phosphate (BCP) from calcium pyrophosphate (CPP) deposition diseases. Pascart et al. compared several dual-energy parameters of presumed CPP deposits contained in meniscal calcinosis to those of presumed BCP both in subchondral trabecular bone and bone plate [3]. The authors found statistically significant differences in dual energy index (DEI), electron density (Rho) and measured effective atomic number (Z_{eff}). For instance they reported a DEI range for meniscal CPP of 0.023 ± 0.007, versus 0.041 ± 0.008 for the subchondral trabecular bone BCP and 0.067 ± 0.007 for the subchondral bone plate BCP [3]. In a different study, the same group reported statistically significant differences in DEI between CPP deposits (0.034 ± 0.005) and BCP (0.041 ± 0.005) contained within a focus of calcific tendinopathy ($p = 0.008$), specifically when comparing

* Corresponding author. Massachusetts General Hospital, Department of Radiology, YAW6044, 32 Fruit Street, Boston MA 02114, USA.
E-mail address: mjarraya@mgh.harvard.edu (M. Jarraya).

https://doi.org/10.1016/j.ocarto.2024.100436
Received 3 October 2023; Accepted 19 January 2024

foci of mineralization with similar CT numbers [4]. The use of DECT and multi-energy CT to discriminate between BCP and CPP deposit diseases has been supported by phantom experiments in which the two crystals were compared at equal (or close) concentrations [4,6,8].

If validated, this application of DECT to differentiate between different types of calcium crystals would have important implications both for clinical practice and research. It would open the way for *in vivo*, non-invasive differentiation between different types of calcium crystal arthropathies. In addition, it would help understand the potential contribution of each type of calcium crystal in the pathogenesis and progression of osteoarthritis (OA) as well as the identification of possible therapeutic target [9]. Although the data is still limited, the concept of characterization of calcium crystals using DECT and multi-energy CT has become more accepted in the rheumatology and radiology literature. For instance, in the recently published consensus definition of CPP deposition disease, an international multidisciplinary working group included a DEI range of 0.016–0.036 in its final definition of CPP deposition disease [10]. Z_{eff} in the range of 8.5–10 was considered in the preliminary definition but not confirmed in the final criteria [10] because of concern for overlap with Z_{eff} of BCP, previously reported to be as low as 9.2[4]. Our aim was to test the hypothesis that DECT can effectively discriminate between physiologic deposition of BCP and pathologic deposition of CPP crystals in a clinical setting.

2. Methods

This study was IRB-compliant. One male participant aged 71 with chronic knee osteoarthritis and radiographically detected chondrocalcinosis (Fig. 1), scheduled for a posterior cruciate-retaining total knee replacement, was consented for this study. Surgical specimens of the medial meniscus, lateral meniscus, medial femoral condyle, lateral femoral condyle, medial tibial plateau, lateral tibial plateau, patella, anterior cruciate ligament, and capsule were separately labeled and placed in different containers.

2.1. Dual energy CT scanning

Specimens were scanned using a DECT Siemens Somatom Force with standard clinical parameters (80/150 kV, FOV: 250, exposure: 165 mAs, slice thickness: 0.6 mm, resolution: 0.488 × 0.488 mm^2).

2.2. Light microscopy

All surgical specimens were examined under light microscopy using hematoxylin and eosin (HE) stain, after decalcification. Decalcification was performed since some specimens contained bone (medial femoral condyle and lateral tibial plateau). CPP was found in only 4 specimens: 1. Medial meniscus, 2. Lateral meniscus, 3. Medial femoral condyle and 4. Lateral tibial plateau. No evidence of BCP deposits was found in any of the examined specimens. The CPP crystals were identified on light microscopy due to their characteristic rhomboid appearance.

2.3. Dual energy CT analysis

Post-processing of DECT images was made using the Rho/Z software in a dedicated workstation (syngo.via VB10B; Siemens Healthineers). The 80 KVp and 150 KVp images were exported and loaded into 3DSlicer 5.2.2 (https://www.slicer.org/) to place regions of interest (ROIs) using the segmentation tool. Two musculoskeletal radiologists (MJ and RB) placed ROIs on different reformats of the surgical specimens using the 80 KVp image. Three ROIs were placed in each of the areas of microscopically proven CPP deposits, i.e., within the medial and lateral menisci, medial femoral condyle, and lateral tibial plateau. BCP of the subchondral plate (C-BCP) was sampled by placing 3 ROIs in the subchondral plates of each of the medial and lateral femoral condyle, and medial and lateral tibial plateaus. BCP of the trabecular bone (T-BCP) was sampled by placing 3 ROIs in the subchondral trabecular bone in each of the medial and lateral femoral condyle and medial and lateral tibial plateaus. A total 36 ROIs were placed by each reader. Given the very small size of the CPP and BCP crystals, the ROI size and placement could not be standardized. The size of the ROIs was variable to ensure absence of volume averaging. Fig. 1 shows examples of placement of the different ROIs in areas of CPP, T-BCP and C-BCP. For each ROI, five DECT parameters were extracted and saved: CT numbers (at 80 and 150 kV), DEI, electron density (Rho), and Z_{eff}.

2.4. Statistical analysis

We considered each individual voxel within the free-drawn ROIs as an individual observation when performing the statistical analysis. Mean and standard deviations were calculated using Python (available from the SciPy package) for each of CPP, T-BCP, C-BCP and Aggregate-BCP (aggregate of T-BCP and C-BCP). Boxplots were used to display the distribution of each parameter.

3. Results

DECT parameters of both readers within different areas of mineralization are shown in Table 1. The range of CT numbers at 80 KVp and 150 KVp, DEI, rho, and Zeff were generally higher than the range of T-BCP, lower than that of C-BCP, and largely overlapping with Aggregate-BCP (aggregate of T-BCP and C-BCP). This trend was consistent for both readers. For instance, the DEI of CPP was 0.12 ± 0.02 for reader 1 and

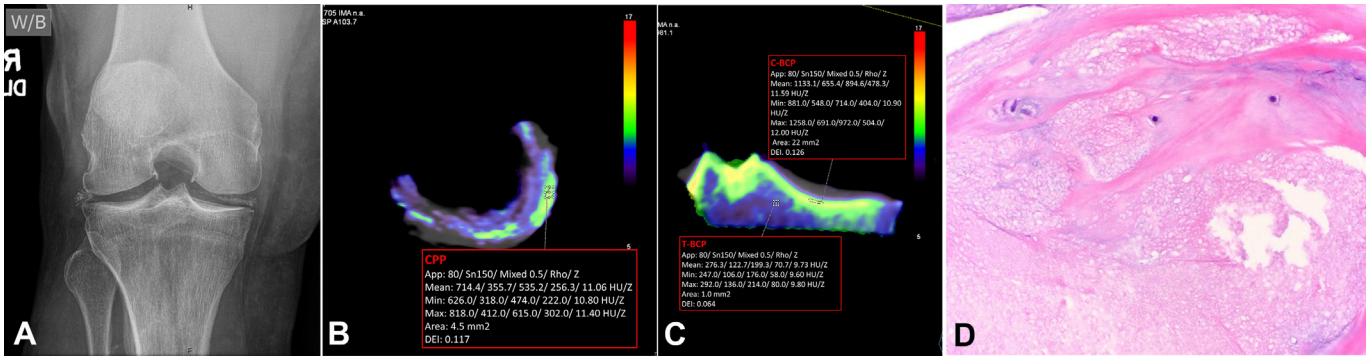

Fig. 1. (A) Preoperative anteroposterior knee radiograph of the study's participant showing meniscal calcinosis with more subtle mineralization of the hyaline cartilage. **(B)** *Ex vivo* DECT axial reformat of the lateral meniscus with an ROI placed in a focus of CPP, as proven by microscopy. **(C)** *Ex vivo* DECT coronal reformat of the lateral tibial plateau, ROI placement in the subchondral cortical bone plate (C-BCP) and within the subchondral trabecular bone (T-BCP). **(D)** Histologic examination of the lateral meniscus. Hematoxylin and eosin staining shows presence of CPP crystals.

Table 1
Mean and standard deviations of CT attenuation values, dual energy index (DEI), electron density (Rho) and effective atomic numbers (Zeff) in trabecular bone (T-BCP), cortical bone (C-BCP), and foci of calcium pyrophosphate (CPP) from both readers. Aggregate-BCP aggregates both T-BCP and C-BCP regions. In each region, 3 ROIs were placed.

READER 1	80 KVp (SD)	150 KVp (SD)	DEI (SD)	Rho (SD)	Z_{eff} (SD)
T-BCP	517.5 (135.9)	235.7 (70.5)	0.10 (0.02)	138.9 (53.1)	10.77 (0.48)
C-BCP	1131.8 (216.0)	614.5 (120.0)	0.14 (0.02)	433.4 (93.0)	11.80 (0.44)
Aggregate-BCP	799.1 (353.7)	409.3 (211.9)	0.12 (0.03)	273.9 (164.4)	11.24 (0.69)
CPP	647.3 (117.2)	293.2 (69.8)	0.12 (0.02)	232.4 (53.6)	10.83 (0.44)
READER 2	80 KVp (SD)	150 KVp (SD)	DEI (SD)	Rho (SD)	Z_{eff} (SD)
T-BCP	426.5 (173.3)	191.4 (92.5)	0.09 (0.03)	114.5 (72.9)	10.32 (0.75)
C-BCP	1251.4 (235.6)	671.1 (143.5)	0.15 (0.01)	475.8 (113.1)	12.03 (0.36)
Aggregate-BCP	625.0 (400.6)	306.9 (231.3)	0.10 (0.04)	201.5 (176.0)	10.73 (1.00)
CPP	485.4 (170.0)	247.0 (84.9)	0.09 (0.03)	186.4 (64.2)	10.11 (0.66)

DEI: Dual energy index, **Rho:** electron density, **Z_{eff}**: effective atomic number. 80 KVp, 150 KVp, and Rho are reported in Hounsfield Units.

0.09 ± 0.03 for reader 2, versus 0.12 ± 0.03 and 0.10 ± 0.04 for Aggregate-BCP, respectively. Rho of CPP was 232.4 ± 53.6 for reader 1 and 186.4 ± 64.2 for reader 2, versus 273.9 ± 164.4 and 201.5 ± 176, for Aggregate-BCP respectively. Finally, Z_{eff} of CPP was 10.83 ± 0.44 for reader 1 and 10.11 ± 0.66 for reader 2, versus 11.24 ± 0.69 and 10.73 ± 1 for Aggregate-BCP, respectively. The overlap between the DECT parameters of CPP and BCP (aggregate of T-BCP and C-BCP) is also illustrated in Fig. 2.

4. Discussion

Our findings largely contradict the consensus definition and prior data on the use of DECT for characterization of calcium crystals. First, we found a DEI of 0.10–0.11 for pathology-proven CPP, which is markedly above the reported range of 0.016–0.036 in the recently published final definition of CPP [10]. Our findings of Z_{eff} of 10.4–10.7 for CPP are also higher than the range of 8.5–10 as published in the preliminary consensus definition of CPP [10]. Moreover, our findings suggest DECT parameters do not allow effectively discrimination between CPP and BCP, considering the large overlap between CPP and Aggregate-BCP. Thus, our findings suggest that the differences of these measurements are dependent on the density (concentration) of calcium rather than a reflection of different elemental composition between CPP and BCP.

The potential use of DECT and multi-energy CT for characterization of calcium crystals and differentiation between BCP and CPP deposit diseases would have an important impact in clinical research, not only to differentiate between different types of calcium crystal arthropathies, but most importantly to understand the role of each calcium crystal in the pathogenesis and progression of OA [9]. This differentiation would have an implication on treatment as well.

In DECT (and CT in general), the material differentiation relies of energy dependence of CT attenuation for different materials. Both Compton scatter and photoelectric effect are the main processes accounting for X-ray attenuation. Unlike Compton scatter, the photoelectric effect is strongly dependent on both X-ray energy and the atomic number of the element being imaged. Thus, photoelectric effect is key for material decomposition based on spectral properties with DECT. However, to differentiate between different materials based on their spectral properties there must be "sufficient" differences in their atomic number or effective atomic numbers [11]. For instance, iodine (Z = 53) and calcium

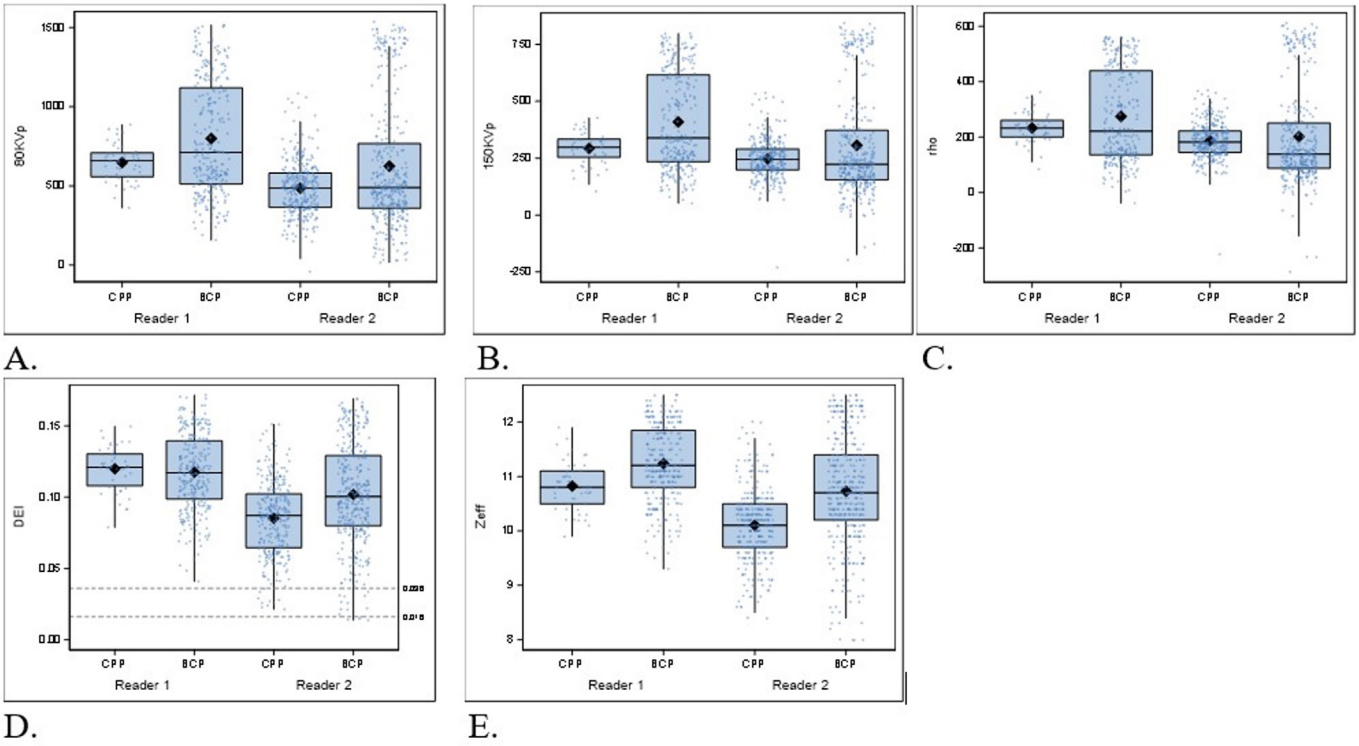

Fig. 2. Box and whisker plots for **A.** CT attenuation values at 80 KVp and **B.** 150 KVp, **C.** dual energy index (DEI), **D.** Electron density (Rho) and **E.** Effective atomic numbers (Z_{eff}) of BCP (which aggregates both BCP within trabecular bone and BCP within cortical bone), and foci of calcium pyrophosphate (CPP) from both readers. Of note figure **D** shows the DEI range if 0.0160–0.036 (dashed lines) as proposed in the final definition of CPP.

(Z = 20) can be differentiated from each other and from materials with lower atomic numbers, such as H, C, N and O, which have atomic numbers varying between 1 and 8. CPP and hydroxyapatite (HA), which is the main BCP of interest, are very similar in terms of Z_{eff} and elemental composition since both contain calcium (Z = 20) and phosphate (Z = 15) atoms. Indeed, the similar molecular formula of calcium pyrophosphate ($Ca_2O_7P_2$) and HA ($Ca_5HO_{13}P_3$) make the physical and chemical properties of these two compounds (Z_{eff} of CPP = 15.24 versus Z_{eff} of HA = 15.86) [12] too close to allow reliable differentiation in terms of X-ray attenuation. It is important to acknowledge that while DEI characterizes the spectral behavior of a given material within a voxel, it is dependent not only on the composition of the material but also the X ray spectrum. On the other hand, Z_{eff} is theoretically a property of the tissue, independent of the scanning protocol [13]. In addition, the electron density is approximately bilinear to the CT number and can be estimated with single-energy CT [14]. The added value of DECT compared to single-energy CT is mainly the measurement of Z_{eff} [15], which are hardly distinguishable between calcium pyrophosphate and HA.

The slight difference in calcium concentration between HA and CPP may explain the differences in CT numbers and other DECT parameters that were previously reported in phantoms at identical concentrations of these two compounds [4,6]. However, we also note that Døssing et al. performed similar measures on phantoms of HA and CPP at equal and different concentrations but did not show any difference between the DECT parameters of these 2 compounds [16]. The authors hypothesized that a large enough size of ROI may be of importance for reliable measurements, however these crystals are often present in small foci limiting use of large ROIs in a clinical setting [16]. Given that the occurrence of pathologic deposition of CPP and BCP often occurs at unknown concentrations, the use of phantoms would not help differentiating between the two substrates. While Multi-energy photon counting CT may enable improved spectral material characterization, in part because of its potential to perform K-edge imaging and classify materials of potential interest at low concentrations, it is worth noting that there is no difference in K-edge between CPP and BCP both of which contains calcium and phosphate atoms [11]. In addition the k-edge of calcium (4.0 keV) is too low to be exploited with current clinical imaging techniques operating in the human energy range [5]. Of note, between reader reliability was outside the scope of this study but can be considered in future studies. In our study the between reader variations are presented in Fig. 2.

Our study has several limitations that should be acknowledged. First, our findings were based on a small number of surgical specimens, all of which were from a single patient. In addition, our study did not account for variations in elemental composition within BCP compounds, since BCP refers to the trio: 1) HA, 2) octacalcium phosphate and 3) tricalcium phosphate. Also, we did not account for the variation between BCP contained in bone and pathologic deposition of BCP in the soft tissues. However, these sources of variability could only make the differentiation between BCP and CPP even more challenging. Future research should focus on comparing pathology proven deposits of CPP and BCP in the soft tissues.

In summary, our findings show that DECT is not appropriate for differentiation between pathologic deposition of CPP and physiologic deposition of BCP in the bone. We demonstrate there is a large overlap of all examined DECT parameters (including for DEI and Z_{eff}) of CPP and BCP, preventing an effective differentiation between the two compounds. The observed differences in DECT parameters between T-BCP, C-BCP and CPP in our work and in prior publications most likely reflect differences in calcium concentration, rather than differences in elemental composition. DECT parameters including DEI should not be used as definition criteria of CPP.

Key result

Dual energy index, electron density and effective atomic number extracted from dual energy CT did not allow differentiation between pathology-proven deposits of calcium pyrophosphate and areas of basic calcium phosphate contained within the trabecular bone and subchondral bone plate.

Summary statement

Calcium pyrophosphate and basic calcium phosphate deposit diseases cannot be differentiated using dual-energy CT.

Authors contribution

Study conception and design: MJ, SY, AG.
Acquisition of data: MJ, RB, OB, EG, CMM, GPN.
Analysis and interpretation of data: MJ, JC, AG, DW, RG, FJS, PO.
Drafting/revising article and approving of final version: All authors.

Funding source

RG is supported by grants 5R01CA212382-05, (PI: Yoshida, Hiroyuki); 5R01EB024343-04, (PI: Bonmassar, Giorgio); and 1R03EB032038-01 (PI: Gupta, Rajiv).

Declaration of competing interest

AG has received consultancies fees from Pfizer, Novartis, AstraZeneca, Coval, Medipost, ICM and TissueGene and is a shareholder of Boston Imaging Core Lab (BICL), LLC a company providing image assessment services. CMM has received consultancy fees from Smith and Nephew. JC has received consultancy fees from Boston Imaging Core Lab.

References

[1] H. Tanikawa, R. Ogawa, K. Okuma, et al., Detection of calcium pyrophosphate dihydrate crystals in knee meniscus by dual-energy computed tomography, J. Orthop. Surg. 13 (1) (2018) 73, https://doi.org/10.1186/s13018-018-0787-0.
[2] T. Diekhoff, T. Kiefer, A. Stroux, et al., Detection and characterization of crystal suspensions using single-source dual-energy computed tomography: a phantom model of crystal arthropathies, Invest. Radiol. 50 (4) (2015) 255–260, https://doi.org/10.1097/RLI.0000000000000099.
[3] T. Pascart, L. Norberciak, J. Legrand, F. Becce, J.F. Budzik, Dual-energy computed tomography in calcium pyrophosphate deposition: initial clinical experience, Osteoarthritis Cartilage 27 (9) (2019) 1309–1314, https://doi.org/10.1016/j.joca.2019.05.007.
[4] T. Pascart, G. Falgayrac, L. Norberciak, et al., Dual-energy computed-tomography-based discrimination between basic calcium phosphate and calcium pyrophosphate crystal deposition in vivo, Ther Adv Musculoskelet Dis 12 (2020) 1759720X20936060, https://doi.org/10.1177/1759720X20936060.
[5] T.E. Kirkbride, A.Y. Raja, K. Müller, C.J. Bateman, F. Becce, N.G. Anderson, Discrimination between calcium hydroxyapatite and calcium oxalate using multienergy spectral photon-counting CT, AJR Am. J. Roentgenol. 209 (5) (2017) 1088–1092, https://doi.org/10.2214/AJR.17.18394.
[6] L.K. Stamp, N.G. Anderson, F. Becce, et al., Clinical utility of multi-energy spectral photon-counting computed tomography in crystal arthritis, Arthritis Rheumatol Hoboken NJ 71 (7) (2019) 1158–1162, https://doi.org/10.1002/art.40848.
[7] I. Bernabei, Y. Sayous, A.Y. Raja, et al., Multi-energy photon-counting computed tomography versus other clinical imaging techniques for the identification of articular calcium crystal deposition, Rheumatol Oxf Engl 60 (5) (2021) 2483–2485, https://doi.org/10.1093/rheumatology/keab125.
[8] A. Viry, A.Y. Raja, T.E. Kirkbride, et al., Multi-energy spectral photon-counting CT in crystal-related arthropathies: initial experience and diagnostic performance in vitro, in: SPIE 10573, 2018, https://doi.org/10.1117/12.2293458.
[9] S. Stücker, M. Bollmann, C. Garbers, J. Bertrand, The role of calcium crystals and their effect on osteoarthritis pathogenesis, Best Pract. Res. Clin. Rheumatol. 35 (4) (2021) 101722, https://doi.org/10.1016/j.berh.2021.101722.
[10] S.K. Tedeschi, F. Becce, T. Pascart, et al., Imaging features of calcium pyrophosphate deposition disease: consensus definitions from an international multidisciplinary working group, Arthritis Care Res. 75 (4) (2023) 825–834, https://doi.org/10.1002/acr.24898.
[11] R. Forghani, B. De Man, R. Gupta, Dual-energy computed tomography: physical principles, approaches to scanning, usage, and implementation: Part 1, Neuroimaging Clin. 27 (3) (2017) 371–384, https://doi.org/10.1016/j.nic.2017.03.002.

[12] T. Henriksen, J. Baarli, The effective atomic number, Radiat. Res. 6 (4) (1957) 415–423.
[13] R.E. Alvarez, A. Macovski, Energy-selective reconstructions in X-ray computerized tomography, Phys. Med. Biol. 21 (5) (1976) 733–744, https://doi.org/10.1088/0031-9155/21/5/002.
[14] U. Schneider, E. Pedroni, A. Lomax, The calibration of CT Hounsfield units for radiotherapy treatment planning, Phys. Med. Biol. 41 (1) (1996) 111–124, https://doi.org/10.1088/0031-9155/41/1/009.
[15] L.I.R. Garcia, J.F.P. Azorin, J.F. Almansa, A new method to measure electron density and effective atomic number using dual-energy CT images, Phys. Med. Biol. 61 (1) (2016) 265–279, https://doi.org/10.1088/0031-9155/61/1/265.
[16] A. Døssing, F.C. Müller, F. Becce, L. Stamp, H. Bliddal, M. Boesen, Dual-energy computed tomography for detection and characterization of monosodium urate, calcium pyrophosphate, and hydroxyapatite: a phantom study on diagnostic performance, Invest. Radiol. 56 (7) (2021) 417–424, https://doi.org/10.1097/RLI.0000000000000756.